Proc. Natl. Acad. Sci. USA
Vol. 93, pp. 8460–8464, August 1996
Developmental Biology

Defective forebrain development in mice lacking gp330/megalin

(cholesterol/apoB/plasminogen activation/lipoprotein transport)

THOMAS E. WILLNOW*†, JAN HILPERT*, SCOTT A. ARMSTRONG*, ASTRID ROHLMANN*, ROBERT E. HAMMER‡§, DENNIS K. BURNS¶, AND JOACHIM HERZ*

Departments of *Molecular Genetics, ‡Biochemistry, and ¶Pathology, and §Howard Hughes Medical Institute, University of Texas Southwestern Medical Center, Dallas TX 75235

Communicated by Marilyn Gist Farquhar, University of California at San Diego, La Jolla, CA, May 7, 1996 (received for review March 6, 1996)

ABSTRACT **gp330/megalin, a member of the low density lipoprotein (LDL) receptor gene family, is expressed on the apical surfaces of epithelial tissues, including the neuroepithelium, where it mediates the endocytic uptake of diverse macromolecules, such as cholesterol-carrying lipoproteins, proteases, and antiproteinases. Megalin knockout mice manifest abnormalities in epithelial tissues including lung and kidney that normally express the protein and they die perinatally from respiratory insufficiency. In brain, impaired proliferation of neuroepithelium produces a holoprosencephalic syndrome, characterized by lack of olfactory bulbs, forebrain fusion, and a common ventricular system. Similar syndromes in humans and animals are caused by insufficient supply of cholesterol during development. Because megalin can bind lipoproteins, we propose that the receptor is part of the maternal–fetal lipoprotein transport system and mediates the endocytic uptake of essential nutrients in the postgastrulation stage.**

gp330/megalin (hereafter referred to as megalin) was originally described as the major autoantigen in an induced glomerular nephritis model in rats and is therefore also known as the Heymann nephritis antigen (1, 2). cDNA cloning revealed that megalin is a member of the low density lipoprotein (LDL) receptor gene family (3), which consists of seven structurally related endocytic receptors (4, 5). Family members also include the LDL receptor (6) and the LDL receptor-related protein (LRP) (7). *In vitro*, megalin binds several of the ligands that interact with LRP, a multifunctional receptor that participates in a number of diverse biological processes including hepatic lipoprotein metabolism and regulation of extracellular protease homeostasis. Ligands common to both receptors are apolipoprotein (apo) E-enriched lipoproteins, lipoprotein lipase, plasminogen activators (PAs), and complexes of PA with their inhibitor PA inhibitor 1 (PAI-1) (8–10). Despite the overlap in ligand binding spectrum, differences in the expression pattern of LRP and megalin suggest important functional differences *in vivo*. LRP is expressed to a variable extent in most tissues including fibroblasts and macrophages, but is most abundant in hepatocytes and neurons (7, 11, 12). In contrast, megalin is primarily found on the apical surfaces of epithelia of the glomerulus and proximal tubule in the kidney, the type II pneumocytes, and Clara cells in the lung and the ependymal cells in the brain (13, 14). During embryonic development megalin is first expressed on the trophoectoderm of preimplantation blastocysts and later in the yolk sac, the amniotic ectoderm, and neuroectoderm (15, 16).

To explore the relevant physiological processes in which megalin participates *in vivo* we have disrupted the gene in mice. Analysis of megalin-deficient animals revealed developmental abnormalities in kidneys, lungs and the central nervous system (CNS), consistent with the expression pattern of the protein. The absence of megalin affects predominantly the development of the forebrain and anterior viscerocranium and structures derived from the rostral parts of the developing neuroepithelium and from adjacent neural crest. This phenotype is consistent with a role of megalin as an endocytic receptor that mediates the cellular uptake of essential nutrients, possibly lipoprotein-derived cholesterol, from the amniotic fluid into the rapidly dividing neuroepithelium before the establishment of a complete circulatory system in the embryo.

EXPERIMENTAL PROCEDURES

Construction of Targeting Vector. A 10-kb *Bam*HI–*Sal*I subfragment and a 1.2-kb PCR product derived from the murine megalin gene were used as short and long homology region and fused to the 5′ and 3′ ends of the *pol2sneobpA* expression cassette, respectively. This results in replacement of 1.5 kb of intermediate genomic sequences including exon sequences 3′ of amino acid Asn-4204 (corresponding rat sequence) by *neo*. Two copies of the herpes simplex virus thymidine kinase gene were inserted in tandem at the 5′ end of the short homology region. Electroporation of the linearized replacement vector into murine embryonic stem cells JH1 and derivation of germ line chimeras from two independent stem cell clones was performed according to standard protocols. The presence of the disrupted allele was confirmed by hybridizing *Hin*dIII and *Bam*HI digested genomic DNA with a 0.8-kb *Sal*I–*Pst*I fragment located 5′ of the short homology region.

Bone and Cartilage Staining of Mouse Embryos. Embryos were obtained by cesarean section at day 18.5 postcoital and euthanized by intraperitoneal injection of pentobarbital sodium. The tip of the tail was clipped for genotyping. Skin and visceral organs were removed and the specimen processed for staining with Alizarin Red S and Alcian Blue as described (17).

Histological Analysis of Lung, Kidney, and Brain Tissues. Newborn mice were sacrificed by decapitation, the lungs were fixed in 10% neutral buffered formalin for 4 days, after which the tissues were processed for paraffin sectioning. The heads were fixed in Bouin's fixative for 1 h first, subsequently cut with a razor blade in coronal orientation once and fixed for additional 1 h, after which they were incubated in 10% neutral buffered formalin for 16 h, followed by paraffin sectioning. Serial paraffin sections of 4–6 μm were cut and every 10th section was stained with hematoxylin and eosin. For electron microscopy, kidneys from newborn mice were fixed in 3% glutaraldehyde, postfixed in osmium tetroxide in phosphate buffer (PB), dehydrated, embedded in Epon, and subjected to sectioning.

The publication costs of this article were defrayed in part by page charge payment. This article must therefore be hereby marked "*advertisement*" in accordance with 18 U.S.C. §1734 solely to indicate this fact.

Abbreviations: LDL, low density lipoprotein; LRP, LDL receptor-related protein; apo, apolipoprotein; PA, plasminogen activator; PAI-1, PA inhibitor 1; CNS, central nervous system; PB, phosphate buffer.

†Present address: MDC, Franz-Gross-Haus/134D, Wiltbergstrasse 50, 13125 Berlin, Germany.

Immunohistochemistry. Day 9.5 embryos were fixed in 3% paraformaldehyde for 2 h at room temperature and then incubated in 20% sucrose in phosphate buffer at 4°C for 16 h. The tissues were processed for frozen sectioning and 10-μm sections were mounted onto polylysine-coated slides. Frozen sections were incubated with polyclonal rabbit anti-rat megalin IgG 612. Bound IgG was detected with goat anti-rabbit antiserum and subsequent incubation with peroxidase-coupled rabbit anti-peroxidase antiserum (Nordic, Lausanne, Switzerland) and detection with diaminobenzidine (peroxidase-antiperoxidsase method). Tissues were counterstained with contrast GREEN (Kirkegaard & Perry). Genotypes were confirmed by Southern blot analysis of yolk sac DNA.

Analysis of Day 8.5 and Day 9.5 Mouse Embryos. For vital dye staining, day 9.5 embryos were dissected from the uterus, incubated in Nile blue sulfate/Ringer solution (1:50,000; wt/vol) for 30 min and rinsed. After photographic documentation, the specimen was used for genotyping by Southern blotting. Scanning electron microscopy of forebrain development was performed on embryos from matings of megalin$^{+/-}$ mice at day 8.5 of gestation. Embryos were dissected from the extraembryonic membranes and fixed in 2.5% glutaraldehyde in 0.1 M PB. Specimens were postfixed in osmium tetroxide, dehydrated, critical point dried, coated with gold-palladium, and mounted at 15 kV on a JEOL scanning electron microscope.

RESULTS

Disruption of the Murine Megalin Gene. Mice in which the megalin gene has been functionally inactivated by homologous recombination were generated by standard procedures. The strategy is shown in Fig. 1 *A* and *B*. Heterozygous offspring of chimeric animals were identified by Southern blot analysis of *Hin*dIII/*Bam*HI-digested tail DNA (Fig. 1*C*) and were superficially indistinguishable from their wild-type littermates. The findings reported in this study were obtained from mice derived from two independently targeted embryonic stem cell clones. Both strains gave identical results.

Megalin-Deficient Pups Die Perinatally. A quarter of the newborn pups obtained from heterozygous matings die perinatally. Of these, ≈50% remain severely cyanotic and die within the first few minutes, apparently due to an inability to breathe despite intensive gasping efforts. The others initially ventilate normally, but within 2–3 h they also die from respiratory insufficiency. These animals were shown to be homozygous for the megalin gene disruption by Southern blotting (Fig. 1*C*, lane 3, −/−). Immunoblot analysis of kidney membrane extracts and urine confirmed the complete absence of the normal protein as well as of any possible truncated protein product in the −/− animals (Fig. 1*D*, lanes 3 and 4). Expression of the receptor-associated protein (RAP), a chaperone for megalin biosynthesis (18, 19) was not affected (data not shown).

Because megalin is expressed in epithelia of the lung, and because megalin$^{-/-}$ newborn mice die from perinatal respiratory complications, we compared the architecture of the lungs of newborn wild type and megalin$^{-/-}$ pups. While the alveoli were uniformly expanded in wild-type animals (Fig. 2*a*), emphysematous areas (characterized by overbloated alveoli) and atelectic areas (characterized by collapse and thickened alveolar walls) marked the lungs of knockout mice (Fig. 2*b*). Thus, impaired pulmonary inflation and alveolar expansion is the likely reason for the respiratory insufficiency and subsequent perinatal death of megalin$^{-/-}$ pups.

Kidney Phenotype. The proximal tubular cells in the kidney are the site of highest megalin expression (2, 13, 14). We therefore examined megalin$^{-/-}$ kidneys for possible structural or functional defects. Light (not shown) and electron microscopical analysis of proximal tubular epithelial cells demonstrated a decreased number and size of large endosomes, also known as apical vesicles, in megalin-deficient cells compared with wild-type cells (Fig. 2 *c* and *d*). These results indicate that megalin is not required for kidney development, but seems to play a central role in endocytotic processes by which the proximal tubular cells take up substrates from the glomerular filtrate.

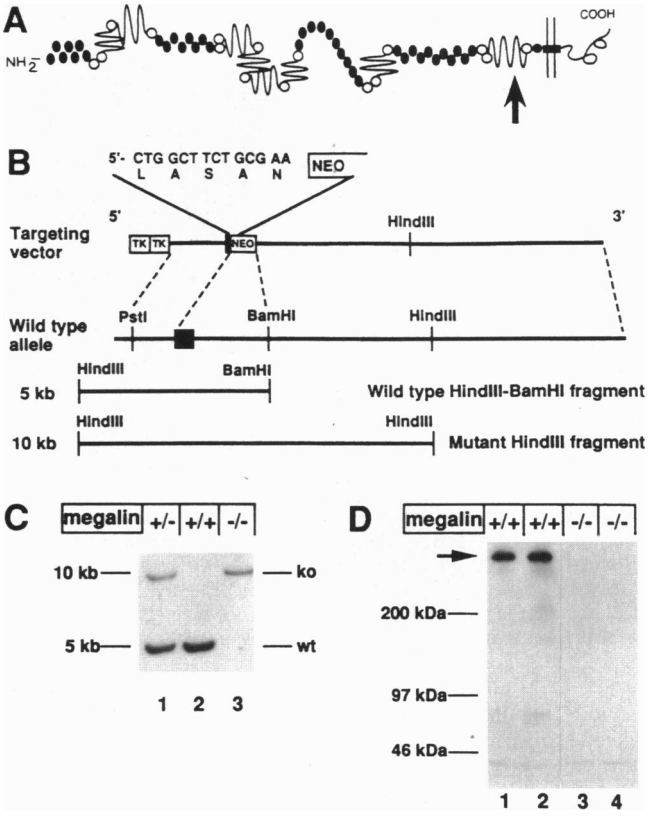

FIG. 1. Gene targeting and characterization of megalin$^{-/-}$ mice by Southern and Western blotting. (*A*) Structure of megalin. Closed ovals: ligand binding-type repeats; open circles: epidermal growth factor-type repeats; filled box: transmembrane segment. Arrow indicates site of gene disruption. (*B*) Replacement vector and targeted disruption of the murine megalin gene. The targeting vector was constructed by replacing ≈1.5 kb of genomic sequences including the 3′ half of an exon (filled box) and part of the downstream intron up to a *Bam*HI restriction site with the *pol2neobp*A cassette (NEO). The DNA and amino acid sequences of megalin preceding the *neo* insertion site are indicated. Two copies of the herpes simplex virus thymidine kinase (TK) gene flank the 5′ homology fragment. Homologous recombination of the targeting vector with the wild-type megalin allele is detected by hybridizing *Hin*dIII and *Bam*HI digested genomic DNA with a probe located 5′ of the *Pst*I restriction site. (*C*) Southern blot analysis of newborn mice. Twenty micrograms of genomic DNA from wild type (+/+, lane 2), heterozygous (+/−, lane 1), and homozygous megalin-deficient mice (−/−, lane 3) was digested with *Bam*HI and *Hin*dIII and subjected to Southern blot analysis as described. DNA fragments diagnostic for the wild type (wt) and the disrupted gene locus (ko) are indicated. (*D*) Immunoblot analysis of kidney membrane proteins. Fifty micrograms of membrane proteins prepared from kidneys of newborn wild-type (lanes 1 and 2) and megalin$^{-/-}$ mice (lanes 3 and 4) was subjected to immunoblot analysis as described (8) by using polyclonal rabbit IgG 612 (5 μg/ml) directed against purified rat megalin and the enhanced chemiluminescence system (ECL; Amersham). Arrow denotes full-length megalin.

Megalin-Deficient Newborns Are Holoprosencephalic. Newborn knockout mice are characterized by the peculiar shape of their heads (Fig. 3*A*). Typical features include a shortened nose and a flattened forehead. Often, a characteristic protrusion is present in the midline of the crown, and in some cases eyes are small (microphthalmia) or absent (anophthalmia) (Fig. 3*A* and Table 1). Further analysis of the underlying brain structures in the −/− newborns revealed an

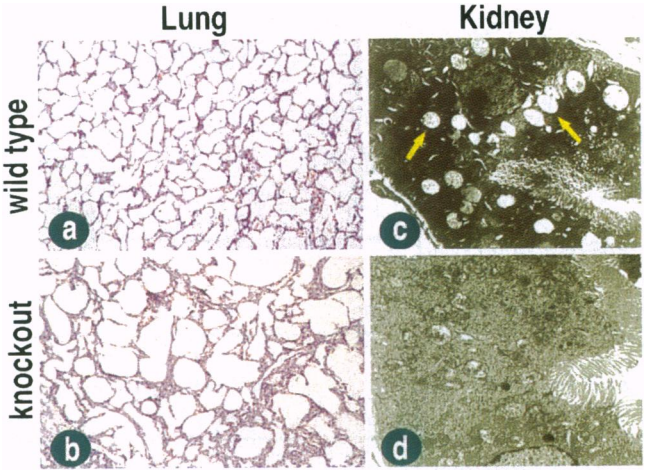

FIG. 2. Lung and kidney histology of wild-type and megalin$^{-/-}$ newborn mice. (*a* and *b*) Paraffin sections (5 μm) of lung tissues obtained from wild-type (*a*) and megalin$^{-/-}$ newborn mice (*b*) stained with hematoxylin and eosin. (×40.) (*c* and *d*) Electron micrograph of cross-sections through proximal tubuli of wild-type (*c*) and knockout kidneys (*d*). Arrows indicate apical vesicles. (×2000.)

almost invariable absence of the olfactory bulbs (Fig. 3*B* and Table 1), accompanied by fusion of the forebrain hemispheres. Alcian/Alizarin stain of cartilage and bone of day 18.5 fetuses (Fig. 3*C*) also revealed a variable degree of dysmorphology of the frontonasal bones in megalin knockouts (specimens 1 and 2), whereas the rest of the skeleton was normally developed. A range of neuroanatomical abnormalities was noted in the knockouts (Fig. 3 *E* and *F* and Table 1), including an almost consistent absence of the corpus callosum. The ventricular system that is normally separated into well-defined lateral (lv) and III ventricles was frequently fused to form a common holoprosencephalic cavity (Fig. 3*F*, hc). Histological analysis revealed the characteristic midline protrusion (Fig. 3*A*) to be caused by a prolaps of choroid plexus (Fig. 3*E*, cp). A high rate of −/− exencephalic newborns was also observed (Table 1).

CNS Expression of Megalin During Development. The neuroanatomical malformations in the megalin$^{-/-}$ mice suggested a manifestation of the gene defect on the level of the neuroepithelium. Consistent with earlier reports that localized

Table 1. Abnormalities of the CNS in megalin$^{-/-}$ newborn mice

Defect	*n*/Total
Absence of corpus callosum	9/10
Microphthalmia/anophthalmia	24/113
Common ventricular system	6/10
Prolaps of choroid plexus	36/73
Dysplasia of olfactory bulbs	16/17
Exencephalus	10/106

n, Number of animals affected; total, number of megalin$^{-/-}$ mice analyzed.

megalin to the ectodermal germ layer in the postimplantation embryo, including the neuroectoderm (15, 16), we found megalin expression to be restricted to the apical surface of the neuroepithelium by immunohistochemical staining of day 9.5 embryos (Fig. 4*A* and *B*). Staining was absent in −/− embryos (Fig. 4*C*). This expression pattern supports a role of megalin in endocytosis of macromolecules from the amniotic fluid that surrounds the neuroepithelium prior to neural tube closure.

Rostral Neuroepithelial Defect. Next, we attempted to determine the specific neuroepithelial cell populations that were affected by the gene defect. Embryos at gestational age day 9.5 were stained *in situ* with Nile Blue, a vital dye that stains apoptotic cells (20) (Fig. 5 *a–c*). Two megalin$^{-/-}$ embryos (Fig. 5 *b* and *c*) are shown in comparison to a wild-type embryo (Fig. 5*a*). At this stage, megalin$^{-/-}$ embryos were visibly smaller than the controls. In each case the size of the telencephalic vesicle (t) was strikingly reduced in the knockouts, whereas the midbrain (m) and hindbrain regions were less affected. Frequently, anterior neural tube closure was delayed in knockout embryos (Fig. 5*c*). In contrast to the low level of apoptosis in the wild type (Fig. 5*a*), pronounced cell death was noted in several areas in the knockout embryos (Fig. 5 *b* and *c*) that corresponded to regions containing facio-acoustic (VII) or trigeminal (V) neural crest, as well as in an area around the optic vesicle (op, II). The latter might explain the variable occurrence of anophthalmia or microphthalmia in the megalin$^{-/-}$ newborns.

The extensive phenotypic changes and cell death that were apparent in the day 9.5 homozygotes suggested that megalin was required for normal viability and development of the neuroepithelium already at an earlier stage. To demonstrate this we analyzed 20 embryos obtained from heterozygous

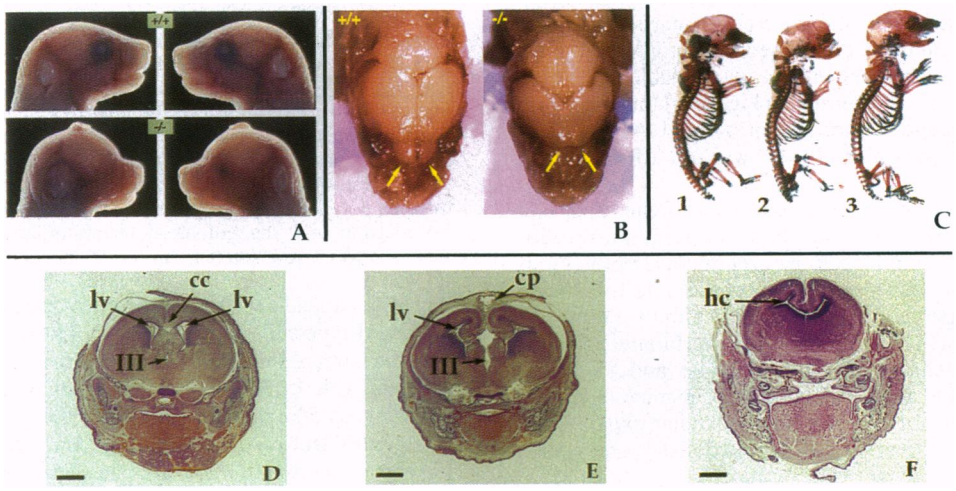

FIG. 3. Craniofacial and brain malformations in megalin-deficient newborn mice. (*A*) Head profiles of wild type (+/+) and megalin-deficient (−/−) newborn mouse. (*B*) Brains of +/+ and −/− mice after removal of the skin and bone. Arrows indicate olfactory bulbs. (*C*) Alizarin Red S/Alcian Blue staining of bone (red) and cartilage (blue) of a wild-type (specimen 3) and two variably affected megalin$^{-/-}$ mouse fetuses at day 18.5 (specimens 1 and 2). (*D–F*) Coronal paraffin sections (5 μm) through the midbrain of a wild-type (*D*) and two megalin$^{-/-}$ newborn mice (*E* and *F*) stained with hematoxylin and eosin. cc, Corpus callosum; cp, protrusion of choroid plexus; lv, lateral ventricle; III, third ventricle; hc, holoprosencephalic cavity. (Bars = 1 mm.)

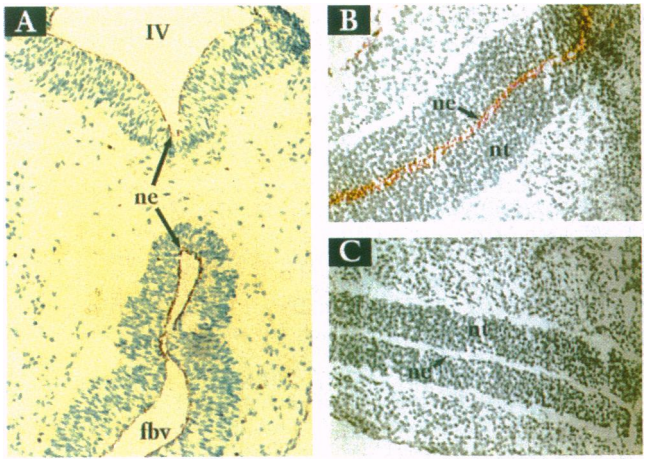

FIG. 4. Immunocytochemical detection of megalin in neuroepithelium of day 9.5 mouse embryos. (*A*) Horizontal section through the head of a wild-type embryo including forebrain vesicle (fbv) and fourth ventricle (IV). (×10.) (*B* and *C*) Section through the neural tube (nt) of wild-type (*B*) and megalin$^{-/-}$ embryo (*C*) in the thoracic region. (×25.) All sections are 10 μm frozen sections. Expression of megalin was detected as described. ne, Neuroepithelium.

matings by scanning electronmicroscopy (Fig. 5 *d–f*). One fourth of these embryos showed distinct dysplastic abnormalities (*) primarily around the region of the forebrain neural folds (fnf). The telencephalon was greatly reduced in size (Fig. 5 *b* and *c*) with an uneven edge of the neural folds (Fig. 5*e*). In some cases, epithelial cohesion was impaired (Fig. 5*f*), resulting in an uneven cobblestone-like neuroepithelial surface and most likely in reduced viability of this rostral neuroepithelial cell population.

DISCUSSION

The present study indicates that megalin is required during the early stages of CNS development in the mouse. Genetic deficiency of this multifunctional receptor results in a holoprosencephalic phenotype, which is characterized by abnormal development of the forebrain, absence of olfactory apparatus, and abnormalities of facial structures that originate from forebrain-derived neural crest and contiguous mesoderm. This phenotype could be the result of cellular starvation for cholesterol and fat-soluble vitamins during the time between gastrulation and neural tube closure when the neuroepithelium may rely on megalin to take up these nutrients from the amniotic fluid.

This hypothesis is supported by several independent lines of evidence. First, megalin is highly expressed on the apical surface of the neuroectoderm and later on the neuroepithelium (ref. 15 and Fig. 4). During the postgastrulation period and before the establishment of an effective circulatory system in the embryo, the nutritional supply of the rapidly dividing neuroepithelium depends on uptake from the surrounding fluids. Before neural tube closure, the apical surface of the neuroepithelium is exposed to the amniotic fluid. Megalin is thus ideally situated to mediate the uptake of cholesterol-rich lipoproteins from the amniotic fluid into this cell population. Several studies have demonstrated that megalin is capable of mediating the cellular uptake of various types of cholesterol-carrying lipoproteins (8, 21, 22).

Second, recent studies suggest that apoB-containing lipoproteins are necessary to deliver cholesterol and fat-soluble vitamins to the developing brain (23, 24). In the embryo, cholesterol and fat-soluble vitamins are taken up from the maternal circulation into the yolk sac. There, the lipids are packaged into lipoproteins containing apoB-100. These lipoproteins are secreted from the yolk sac, and they eventually

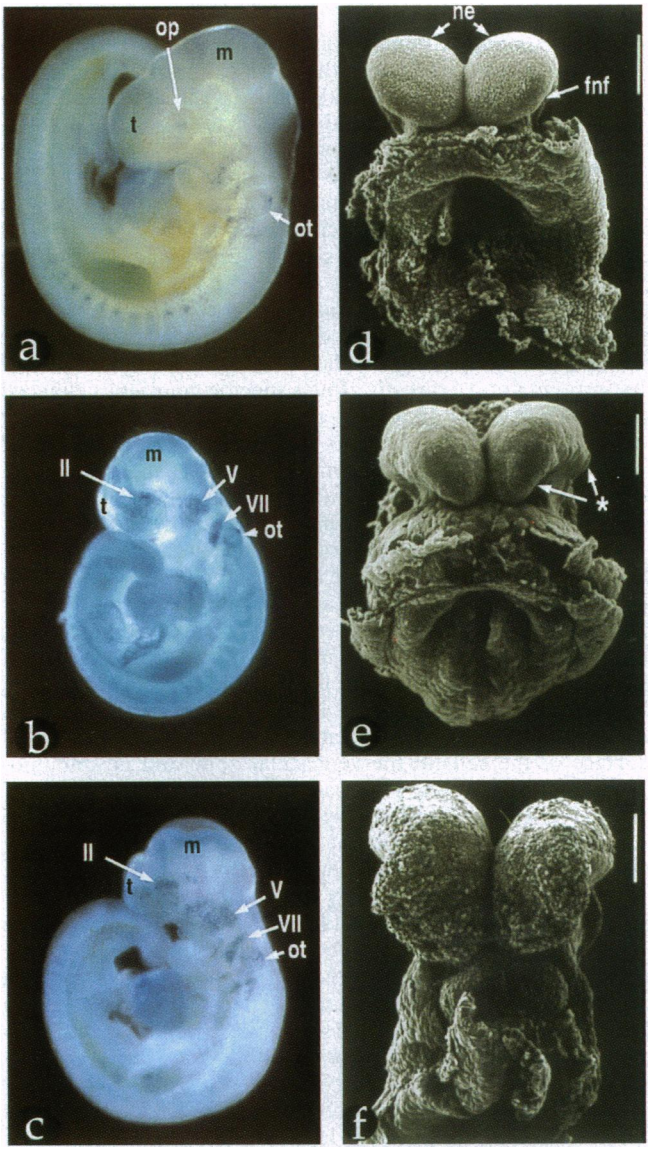

FIG. 5. Analysis of day 8.5 and day 9.5 mouse embryos. (*a–c*) Nile blue staining of day 9.5 wild-type (*a*) and megalin$^{-/-}$ mouse embryos (*b* and *c*). op, Optic vesicle; ot, otic vesicle; m, midbrain; t, telencephalon; II, perioptic neural crest and mesoderm; V, trigeminal ganglion; VII, facio-acoustic ganglion. (*d–f*) Scanning electron microscopy of forebrain development in day 8.5 embryos. The asterisk (*e*) indicates dysplastic forebrain neural folds (fnf); ne, neuroepithelium. (Bars in *d–f* = 200 μm.)

reach the surfaces of the embryonic tissues by diffusion. In mice that are deficient for apoB-100 the yolk sac cannot secrete lipoproteins. These animals die almost invariably during midgestation, with general failure of neural development and extremely low levels of the lipophilic vitamin α-tocopherol (vitamin E) in their tissues (23). Partial inactivation of the apoB gene (24) results in a mitigated phenotype that is also characterized by abnormal neural development including neural tube closure defects, exencephaly and anencephaly. In these mice, enhanced cell death has been demonstrated within a region of the neuroepithelium around gestational day 9 (20).

In addition to uptake from lipoproteins, the developing brain also synthesizes large amounts of cholesterol (25). Administration of the drug AY9944 to rats produces a holoprosencephalic syndrome (26) similar to the one seen in megalin-deficient mice. This compound inhibits 7-dehydrocholesterol-Δ^7-reductase, a late enzyme in the cholesterol biosynthetic pathway, and thus prevents the cells from synthe-

sizing their own cholesterol. The same enzyme is defective in humans with Smith–Lemli–Opitz syndrome (SLO), a recessive genetic disease that includes the holoprosencephalic complex (27). The phenotypic similarities between SLO and megalin-deficiency suggest that in both cases starvation of neuroepithelial cells for cholesterol may be the underlying cause of the malformations. In contrast to mice, the CNS develops normally in human apoB-deficient patients suggesting a variable dependence of different species on endogenous cholesterol synthesis and the exogenous supply of lipids and fat-soluble vitamins during embryonic development.

Our findings suggest that megalin is required for normal cholesterol transport into the developing embryo. The experiments do not yet distinguish, however, to what degree reduced lipoprotein uptake directly affects specific neuroepithelial cell populations in the knockout mice, whether the absence of megalin in the yolk sac also results in reduced uptake of cholesterol from the maternal circulation and whether a combination of these direct and indirect mechanisms might be responsible for the observed phenotype.

Another mechanism that could contribute to the neurodevelopmental defect seen in the knockout mice may result from the functions of megalin in the homeostasis of extracellular proteases. Conceivably, failure to properly regulate proteolytic activity at the cell surface might affect the migration of postmitotic neuroepithelial cells to the higher cortical layers. This alternative mechanism is less likely, however, as megalin expression is highly polarized and restricted to the apical surface of the cells in the ventricular zone and no immunohistochemical staining is apparent in migrating cell populations (Fig. 4). Furthermore, electron microscopical analysis of day 8.5 embryos suggests that expansion and viability rather than migration of the neuroepithelial cells in the forebrain region are directly affected by the megalin gene defect.

An imbalance in extracellular proteolysis may, however, be responsible for the structural abnormalities in megalin-deficient lungs. Increased extracellular proteolytic activity in the lung with analogous structural changes as those seen in megalin knockout mice occurs [e.g., in α_1-antiproteinase deficiency (28) and in transgenic mice that overexpress collagenase (29)].

Megalin was originally discovered as the major antigen in Heymann nephritis and was later found to be an endocytic receptor (1, 30). Our analysis of kidney epithelial cells emphasizes this function by demonstrating a dramatic reduction in the number of endocytic apical vesicles in the knockout animals (Fig. 2). This suggests that megalin is the predominant receptor responsible for endocytic uptake of macromolecules from the apical surface of the proximal tubular cells. This finding further supports the postulated role of megalin as a high capacity transport receptor for essential nutrients during the postgastrulation phase.

We are indebted to K. Sulik for the scanning electron microscopical analysis, and to W.-L. Niu, T. Burnett, and L. Dean for expert technical assistance. This work was supported by grants from the National Institutes of Health (HL 20948), the Keck Foundation, the Perot Family Foundation, and the Lucille P. Markey Charitable Trust. T.E.W. and A.R. were supported by a postdoctoral fellowship from the Deutsche Forschungsgemeinschaft and J. Hilbert was supported by a fellowship from the Deutscher Akademischer Austauschdienst.

1. Kerjaschki, D. & Farquhar, M. G. (1982) *Proc. Natl. Acad. Sci. USA* **79,** 5557–5561.
2. Kerjaschki, D. & Farquhar, M. G. (1983) *J. Exp. Med.* **157,** 667–686.
3. Saito, A., Pietromonaco, S., Loo, A. K.-C. & Farquhar, M. G. (1994) *Proc. Natl. Acad. Sci. USA* **91,** 9725–9729.
4. Krieger, M. & Herz, J. (1994) *Annu. Rev. Biochem.* **63,** 601–637.
5. Schonbaum, C. P., Lee, S. & Mahowald, A. P. (1995) *Proc. Natl. Acad. Sci. USA* **92,** 1485–1489.
6. Yamamoto, T., Davis, C. G., Brown, M. S., Schneider, W. J., Casey, M. L., Goldstein, J. L. & Russell, D. W. (1984) *Cell* **39,** 27–38.
7. Herz, J., Hamann, U., Rogne, S., Myklebost, O., Gausepohl, H. & Stanley, K. K. (1988) *EMBO J.* **7,** 4119–4127.
8. Willnow, T. E., Goldstein, J. L., Orth, K., Brown, M. S. & Herz, J. (1992) *J. Biol. Chem.* **267,** 26172–26180.
9. Christensen, E. I., Gliemann, J. & Moestrup, S. K. (1992) *J. Histochem. Cytochem.* **40,** 1481–1490.
10. Kounnas, M. Z., Chappell, D. A., Strickland, D. K. & Argraves, W. S. (1993) *J. Biol. Chem.* **268,** 14176–14181.
11. Wolf, B. B., Lopes, M. B. S., VandenBerg, S. R. & Gonias, S. L. (1992) *Am. J. Pathol.* **141,** 37–42.
12. Moestrup, S. K., Gliemann, J. & Pallesen, G. (1992) *Cell Tissue Res.* **269,** 375–382.
13. Kounnas, M. Z., Haudenschild, C. C., Strickland, D. K. & Argraves, W. S. (1994) *In Vivo* **8,** 343–352.
14. Zheng, G., Bachinsky, D. R., Stamenkovic, I., Strickland, D. K., Brown, D., Andres, G. & McCluskey, R. T. (1994) *J. Histochem. Cytochem.* **42,** 531–542.
15. Buc-Caron, M. H., Condamine, H. & Kerjaschki, D. (1987) *Ann. Inst. Pasteur/Immunol.* **138,** 707–722.
16. Gueth-Hallonet, C., Santa-Maria, G., Verroust, P. & Maro, B. (1994) *Development (Cambridge, U.K.)* **120,** 3289–3299.
17. McLeod, M. J. (1980) *Teratology* **22,** 299–301.
18. Orlando, R. A., Kerjaschki, D., Kuihara, H., Biemesderfer, D. & Fraquhar, M. G. (1992) *Proc. Natl. Acad. Sci. USA* **89,** 6698–6702.
19. Willnow, T. E., Rohlmann, A., Horton, J., Otani, H., Braun, J. R., Hammer, R. E. & Herz, J. (1996) *EMBO J.* **15,** 2632–2639.
20. Homanics, G. E., Maeda, N., Traber, M. G., Kayden, H. J., Dehart, D. B. & Sulik, K. K. (1995) *Teratology* **51,** 1–10.
21. Stefansson, S., Chappell, D. A., Argraves, K. M., Strickland, D. K. & Argraves, W. S. (1995) *J. Biol. Chem.* **270,** 19417–19421.
22. Kounnas, M. Z., Loukinova, E. B., Stefansson, S., Harmony, J. A., Brewer, B. H., Strickland, D. K. & Argraves, W. S. (1995) *J. Biol. Chem.* **270,** 13070–13075.
23. Farese, R. V., Ruland, S, L., Flynn, L. M., Stokowski, R. P. & Young, S. G. (1995) *Proc. Natl. Acad. Sci. USA* **92,** 1774–1778.
24. Homanics, G. E., Smith, T. J., Zhang, S. H., Lee, D., Young, S. G. & Maeda, N. (1993) *Proc. Natl. Acad. Sci. USA* **90,** 2389–2393.
25. Dietschy, J. M., Kita, T., Suckling, K. E., Goldstein, J. L. & Brown, M. S. (1983) *J. Lipid Res.* **24,** 469–480.
26. Roux, C., Horvath, C. & Dupuis, R. (1979) *Teratology* **19,** 35–38.
27. Tint, G. S., Irons, M., Alias, E. R., Batta, A. K., Frieden, R., Chen, T. S. & Salen, G. (1994) *N. Engl. J. Med.* **330,** 107–113.
28. Cox, D. W. (1989) in *The Metabolic Basis of Inherited Disease*, eds. Scriver, C. R., Beaudet, A. L., Sly, W. S. & Valle, D. (McGraw–Hill, New York), pp. 2409–2435.
29. D'Armiento, J., Dalal, S. S., Okada, Y., Berg, R. A. & Chada, K. (1992) *Cell* **71,** 955–961.
30. Biemesderfer, D., Dekan, G., Aronson, P. S. & Farquhar, M. G. (1992) *Am. J. Physiol.* **262,** F55–F67.